9

Novel Titanium Manganese Alloys and Their Macroporous Foams for Biomedical Applications Prepared by Field Assisted Sintering

Faming Zhang and Eberhard Burkel
Physics of New Materials, University of Rostock
August Bebel Str.55, 18055 Rostock
Germany

1. Introduction

In this chapter, a novel titanium (Ti) alloy and foam suitable for biomedical applications will be introduced. As we know, Ti and its alloys are widely used as biomaterials especially for orthopedic implants in load bearing sites as dental and orthopedic implants and heart valves, due to their high mechanical properties, corrosion resistance and biocompatibility (Geetha et al., 2009). Pure Ti was once used as biomaterial, but its disadvantage as implant materials is low strength and insufficient hardness. Therefore, the Ti6Al4V alloy is preferentially in clinical use because of its favourable mechanical properties. However, some studies showed that the vanadium (V) and aluminium (Al) release in Ti6Al4V alloy could induce Alzheimer's disease, allergic reaction and neurological disorders (Mark & Waqar, 2007). Therefore, the exploration of high strength new Ti alloys without Al and V for medical implants has gained great attention in the past years and it is still ongoing. Al and V free alloys containing non-toxic elements such as iron (Fe), niobium (Nb), zirconium (Zr), tantalum (Ta), molybdenum (Mo), nickel (Ni), gold (Au), or silicon (Si), etc. were investigated (Zhang, Weidmann et al, 2010). As long-term load-bearing implants in clinic, the incorporation of porous structures into the Ti and its alloys could lead to a reliable anchoring of host tissue into the porous structure, and allow mechanical interlocking between bone and implant (Li et al, 2005). The porous structure is preferable for Ti and its alloys used as bone implants. Many techniques have been applied to produce Ti foams in recent years. Nevertheless, there are still problems to be solved in the field of Ti foams for biomedical applications (Zhang, Otterstein et al., 2010): the difficulty to create controlled porosity and pore sizes, the insufficient knowledge of porous structure-property relationships, the requirements of new sintering techniques with rapid energy transfer and less energy consumption and so on.

The Ti alloys and foams are difficult to be produced from the liquid state due to high melting point, high reactive activity at high temperature above 1000 ^{o}C and contamination susceptibility. The production of Ti alloys and foams via a powder metallurgy (PM) route is attractive due to the ability to produce net-shaped components. Because of their stable

surface oxide film (TiO_2), the Ti alloys are difficult to be sintered by traditional PM sintering techniques. Thus, the spark plasma sintering (SPS), a pulsed electric current field assisted sintering technique has been introduced to prepare the Ti alloys. Spark plasma sintering, commonly also defined as field assisted sintering (FAST) or pulsed electric current sintering (PECS) is a novel pressure assisted pulsed electric current sintering process utilizing ON-OFF DC pulse energizing. Due to the repeated application of an ON-OFF DC pulse voltage and current between powder materials, the spark discharge point and the Joule heating point (local high temperature-state) are transferred and dispersed to the overall specimen (Munir & Anselmi-Tamburini, 2006). The SPS process is based on the electrical spark discharge phenomenon: a high energetic, low voltage spark pulse current momentarily generates spark plasma at high localized temperatures, from several to ten thousand degrees between the particles resulting in optimum thermal and electrolytic diffusion. During SPS treatment, powders contained in a die can be processed for diverse novel bulk material applications, for example nanostructured materials (Gao et al., 1999), functional gradated materials (Lou et al., 2003), hard alloys (Zhang et al., 2004), biomaterials (Gu et al., 2004), porous ceramics (Jayaseelan et al., 2002) and diamonds (Zhang et al., 2005) etc. The research group of the author (E.B) has applied the SPS technique also for the synthesis of new materials such as nanostructured magnets, quasicrystals, nanoceramics and Ti alloys (Nicula, Cojocaru et al., 2007; Nicula, Turquier, et al., 2007; Nicula, Lüthen et al., 2007).

The preparation of dense Ti alloys by using the SPS was reported extensively, but still fewer studies were on porous Ti foams (Zhang, Otterstein et al, 2010). The SPS studies on porous Ti alloys were mainly using low temperature and low pressure to decrease the relative density of samples. The samples exhibited pore sizes of some tens of micrometers and a porosity in the range of 20-45%. As bone foams, high porosity (>50%) and macropore size (>200 μm) are essential requirements for the bone growth and the osteoconduction.

We aim at

1. the exploration of new elements within Ti alloys for biomedical applications,
2. the development of new methods to prepare Ti foams for biomedical applications,
3. the deep understanding of the relationships between the microstructure and properties of the new Ti alloy and foams.

Manganese (Mn) is one of the essential trace elements in human body. In recent decades research has discovered the special role manganese plays as a co-factor in the formation of bone cartilage and bone collagen, as well as in bone mineralization (Brown, 2006). The Mn is also beneficial to the normal skeletal growth and development. It is important for enzymes in the body like the superoxide dismutase and, therefore, involved in the elimination of radicals (Zhang, Weidmann et al., 2010). Titanium-manganese (TiMn) alloys have been extensively used in aerospace and hydrogen storage, but not yet in biomedicine. The results in our group showed that the Mn incorporation into the Ti-Al-V alloy could enhance the cell adhesion properties (Nicula, Lüthen et al., 2007). In this chapter, the Mn element was incorporated into the Ti system and TiMn alloys with different Mn amounts were prepared by SPS technique. The preparation process, microstructures, mechanical properties, cytotoxicity and cell proliferation properties of the TiMn alloys were investigated for exploration of their biomedical applications. Macroporous Ti foams with controlled architectures were also prepared using the SPS technique and subsequently modified with TiO_2 nanostructures. The relationship between the properties and the porous architectures was analyzed and discussed.

2. Major raw materials and methods

- The precursor Ti and Mn powders with purities above 99.0% were obtained from Alfa Aesar, Germany. The space holder materials for preparation of Ti foams with 99.0% purity were also obtained form Alfa Aesar and sieved in the range of 100 to 1000 µm.
- The mechanical alloying of the alloy powders is completed using a high energy planetary ball milling machine (Retsch PM400, Germany). The SPS experiments were performed using a Model HPD-25/1 FCT spark plasma sintering system (FCT systeme GmbH, Rauenstein, Germany).
- The analysis of the phase transformation of the alloys was conducted with a differential scanning calorimetry (DSC, DSC 404 C Pegasus®, Germany). The microstructure analysis was performed using X-ray diffraction (XRD, Bruker D8, Germany) and Scanning electron microscopy (SEM, Zeiss Supra 25, Germany). The Ti foam architecture was examined by using X-ray microcomputed tomography (Micro-CT, GE, USA).
- The hardness and the elastic modulus of the dense alloys were measured by Universal CETR Nano+Micro tester with a model UNMT-1 multi-specimen test system. The mechanical behaviour of the Ti foams was investigated by uniaxial compression experiments at room temperature. The plateau stress and further elastic modulus measurements were carried out on a universal testing machine Zwick Roell Z050.
- The human osteoblastic cells MG-63 (osteosarcoma cell line, ATCC, LGC Promochem) were used to investigate the in vitro biocompatibility of the TiMn alloys. The cytotoxicity of the alloys were measured by the methyltetrazolium salt (3-(4,5-dimethylthiazol-2-yl)-5 -(3-carboxy -methoxyphenyl)) (MTS) method. The flow cytometry for determining the cells proliferation property on the alloys was also performed.
- The surface modification of the Ti foams was conducted by soaking in a strong alkali solution and heat treatment. The in vitro bioactivity of the modified foams was tested using a simulated body fluid solution in a shaking bath kept at 37.0 °C.

3. Titanium Manganese alloys

3.1 Phase diagram of the TiMn alloys

The binary phase diagram of TiMn alloys is shown in Fig. 1. It shows the conditions at which thermodynamically distinct phases can occur in equilibrium. The TiMn alloy powders were designed by varying the amount of Mn in the Ti with 2, 5, 8 and 12 (wt.%) compositions on the base of phase diagram. In Fig. 1, the locations of the phases of the Ti-2, 5, 8, 12 wt.% Mn alloys discussed in this work are indicated as straight lines in the phase diagram. The phase compositions of the TiMn alloys with Mn below 12 wt.% are all Ti2Mn2 phase.

3.2 Preparation of the TiMn alloys

The TiMn alloy powders with 2, 5, 8 and 12 wt.% Mn compositions were mixed and mechanical alloyed for various hours in a high energy ball milling machine. Fig. 2 shows the XRD patterns of the pure Ti and Mn powders and of the TiMn alloy powders after 60 hours mechanical alloying. The pure Ti and Mn peaks completely disappeared and TiMn phases

were formed after 60 hours of mechanical alloying. The pure Ti powders show the α-Ti phase (PDF# 65-3362) with hexagonal structure and the pure Mn powders the α-Mn phase (PDF# 32-0637) with cubic structure. The synthesized TiMn powders contain the α-TiMn phase (PDF# 07-0132) with tetragonal structure. There are no obvious changes in the phase compositions with increasing Mn amount up to 12 wt% in Ti, which corresponds to the binary phase diagram of the TiMn alloy (Fig. 1). The powders are analyzed by SEM revealing agglomerates with mean particle sizes of 4-5 μm in diameter with a narrow size distribution. The EDX spectra indicate that the Ti, Mn peaks belong to the TiMn powder. The C and O peaks are resulting from adsorption of air, and the small Fe peak is due to the contamination from the steel balls and vials during the mechanical alloying.

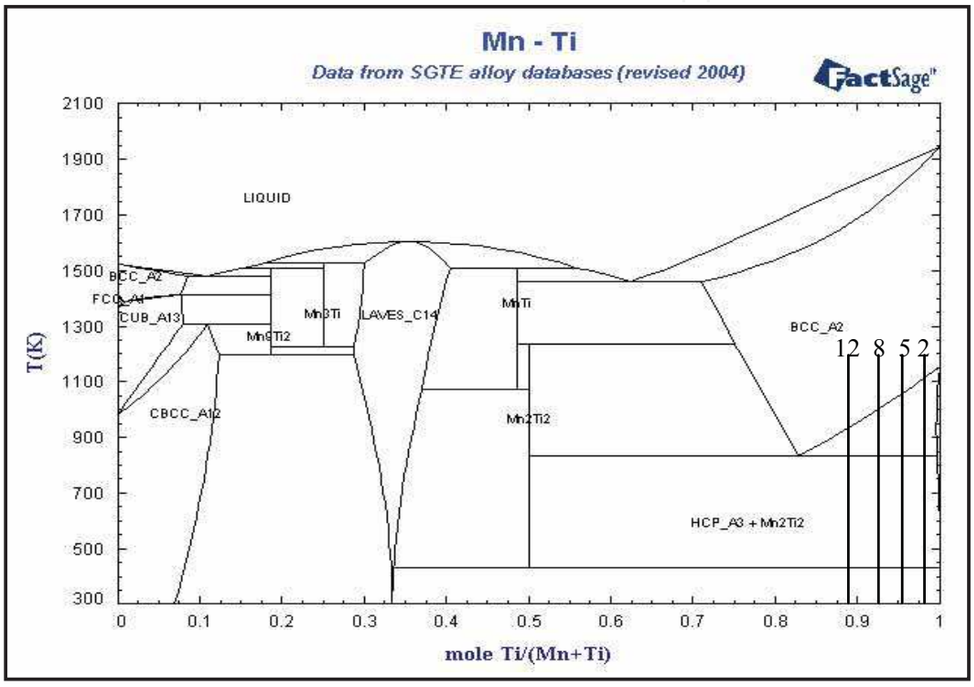

Fig. 1. Binary phase diagram of TiMn alloy showing the phases of the Ti-2, 5, 8, 12 wt.% Mn alloys.

The phase transformation behaviors of the TiMn alloy powders were analyzed by using differential scanning calorimetry. Fig. 3 shows the transformation temperatures of the TiMn alloys in comparison with the pure Ti. In the case of pure Ti, the transformation temperature from α to β phase occurs at about 840 ºC. The transformation temperature in Ti2Mn is at about 735 ºC while that of the Ti5Mn alloys is at about 700 ºC. The transformation temperatures are at about 665 ºC and at about 660 ºC in Ti8Mn and Ti12Mn alloys, respectively. With increasing amount of Mn, the transformation temperature decreased to a lower temperature value. The addition of Mn in Ti has depressed the transformation temperature from the α to the β phase. The elements V, Mo, Nb, Fe, Cr, etc are all β stabilizers and an addition of these elements depresses the β transition temperature. The results in Fig. 3 show that the Mn has decreased the transformation temperature from the α to the β phase. The influence of manganese on the α to β transition temperature is significant. It is confirmed that the Mn is a β stablizing addition element for Ti metals.

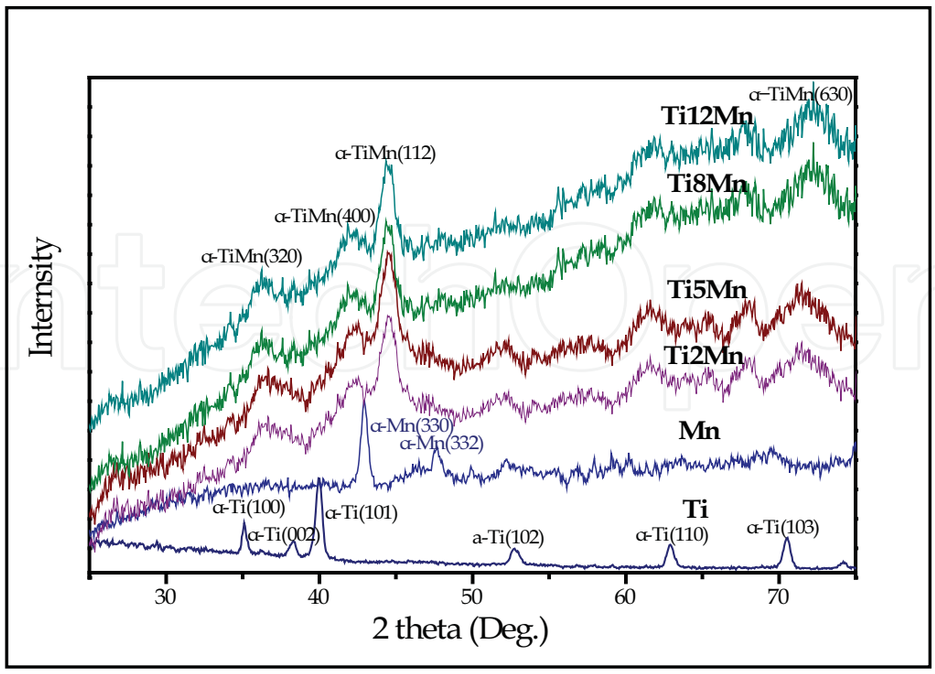

Fig. 2. XRD patterns of the Ti, Mn powders, and TiMn alloy powders prepared by mechanical alloying showing the formation of α-TiMn phases.

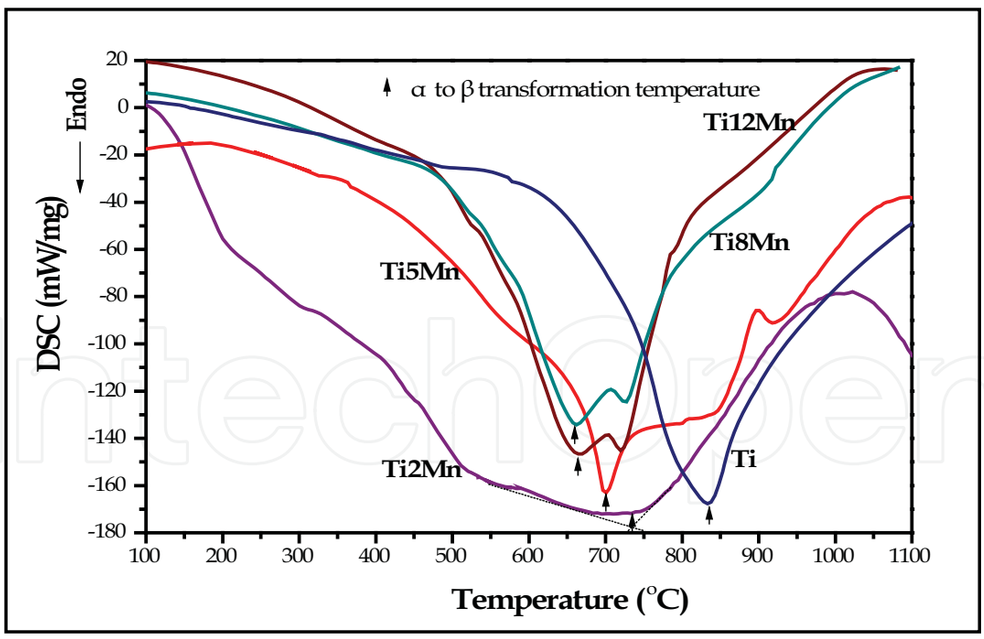

Fig. 3. Phase transformation behaviours of the TiMn alloys measured by DSC showing the decrease of the α to β transformation temperatures with increasing Mn amount.

After characterization, the alloy powders were subjected to the SPS furnace. The relative densities of the spark plasma sintered pure Ti at different temperatures and the TiMn alloys with various Mn amounts were also investigated. With a temperature increase from 550°C

to 800°C, the relative density of the Ti metal increased from 68% to 99%. The relative density of the TiMn alloys increased with higher Mn amount. The Ti8Mn alloys showed 99% relative density after sintering at 700°C for 5 min. The SPS method reduces the sintering temperature of Ti and TiMn alloys. The Mn addition increased the relative density of Ti metal during the SPS treatment. Finally, high density Ti metal was prepared by using the SPS application at 750°C for 5 min and high density TiMn alloys were sintered at 700°C with a holding time of 5 min. By using the traditional sintering techniques, high temperatures of 1100-1300°C would be required to get pure or alloyed high density Ti. The SPS has decreased the sintering temperature of Ti and TiMn alloys. The Mn has increased the relative density of Ti alloy, which is due to the lower β transformation temperatures in the TiMn alloys. The low sintering temperature is ascribed to the ionization of particles by local sparks during SPS. Pulsed current generated plasmas are expected to lead surface activation of the powder particles, melting the titanium oxide films and forming neck junctions among powder particles at a lower temperature (Zhang, Weidmann, 2009).

3.3 Microstructures of the TiMn alloys

Fig. 4 (a) shows X-ray diffraction (XRD) patterns of the spark plasma sintered Ti, Mn and TiMn samples. The pure Ti and Mn still retain the α-Ti and the α-Mn phases because of the lower sintering temperature of 700°C during the SPS treatment. However, most of the TiMn alloys show the β-TiMn phase (PDF# 11-0514) with cubic structure. There is still a small amount of the α-TiMn phase in the alloy; therefore, the TiMn sample is an α+β phase alloy. The synthesized alloy has α+β microstructures which are similar to those of an Ti6Al4V alloy.

The SEM micrograph of the fracture surface of the spark plasma sintered Ti8Mn sample is shown in Fig.4 (b). There are very few micropores in the fracture surface of the TiMn alloys. The grain size of the Ti8Mn alloys is about 500 nm indicating an ultrafine microstructure and the fracture mode of the alloy is primary intergranular cracking. During the SPS, a simultaneous pressure impact causes a plastic flow of the powders, which enables the creation of the dense Ti alloys with ultrafine microstructures at high heating rates, lower temperature and short holding time.

3.4 Properties of the TiMn alloys

The mechanical properties of the TiMn alloys are shown in Fig. 5. The microindentation hardness results show that the hardness value tended to rise with increasing Mn contents (Fig. 5a). The hardness values of all TiMn alloys are significantly higher than that of pure Ti. The pure Ti shows a hardness of 1.60 GPa ± 0.20 GPa; Ti2Mn 2.40 GPa ± 0.25 GPa; Ti5Mn 3.65 GPa ± 0.29 GPa; Ti8Mn 4.98 GPa ± 0.32 GPa and Ti12Mn 5.28 GPa ± 0.37 GPa. The detected hardness value (5.28 GPa ± 0.37 GPa) of the Ti12Mn alloy is comparable to that of the pure Mn (5.44 GPa ± 0,34 GPa). From statistical analysis, the hardness values of the TiMn alloys are significantly higher than that of pure Ti. The elastic modulus results are shown in Fig. 5(b). The pure Ti is 105.3 GPa ± 6.0 GPa, Ti2Mn 83.3 GPa ± 3.0 GPa, Ti5Mn 95.0 GPa ± 5.0 GPa, Ti8Mn 106 GPa ± 4.1 GPa, and Ti12Mn 122 GPa ± 6.2 GPa, Mn 68.72 GPa ± 4.3 GPa. The ductility results of the TiMn alloys are shown in Fig. 5 (c). The pure Ti exhibits 25.0% ± 2.0% ductility, Ti2Mn 21.3% ± 2.4%, Ti5Mn 18.2% ± 2.2%, Ti8Mn 15.0% ± 1.3% and Ti12Mn 11.7% ± 1.9%. The ductility decreased with increasing Mn amounts in the TiMn alloy. For comparison, the mechanical properties of the Ti6Al4V

alloy were also measured with the same methods. This shows a hardness of 4.3 GPa ± 0.3 GPa, an elastic modulus of 122 GPa ± 4.0 GPa, and a ductility of 14.0 GPa ± 1.5 GPa which are almost identical with reported literature values (Barbieri et al., 2007). The Ti2Mn, Ti5Mn and Ti8Mn alloys possess lower elastic modulus and higher ductility than the Ti6Al4V alloy.

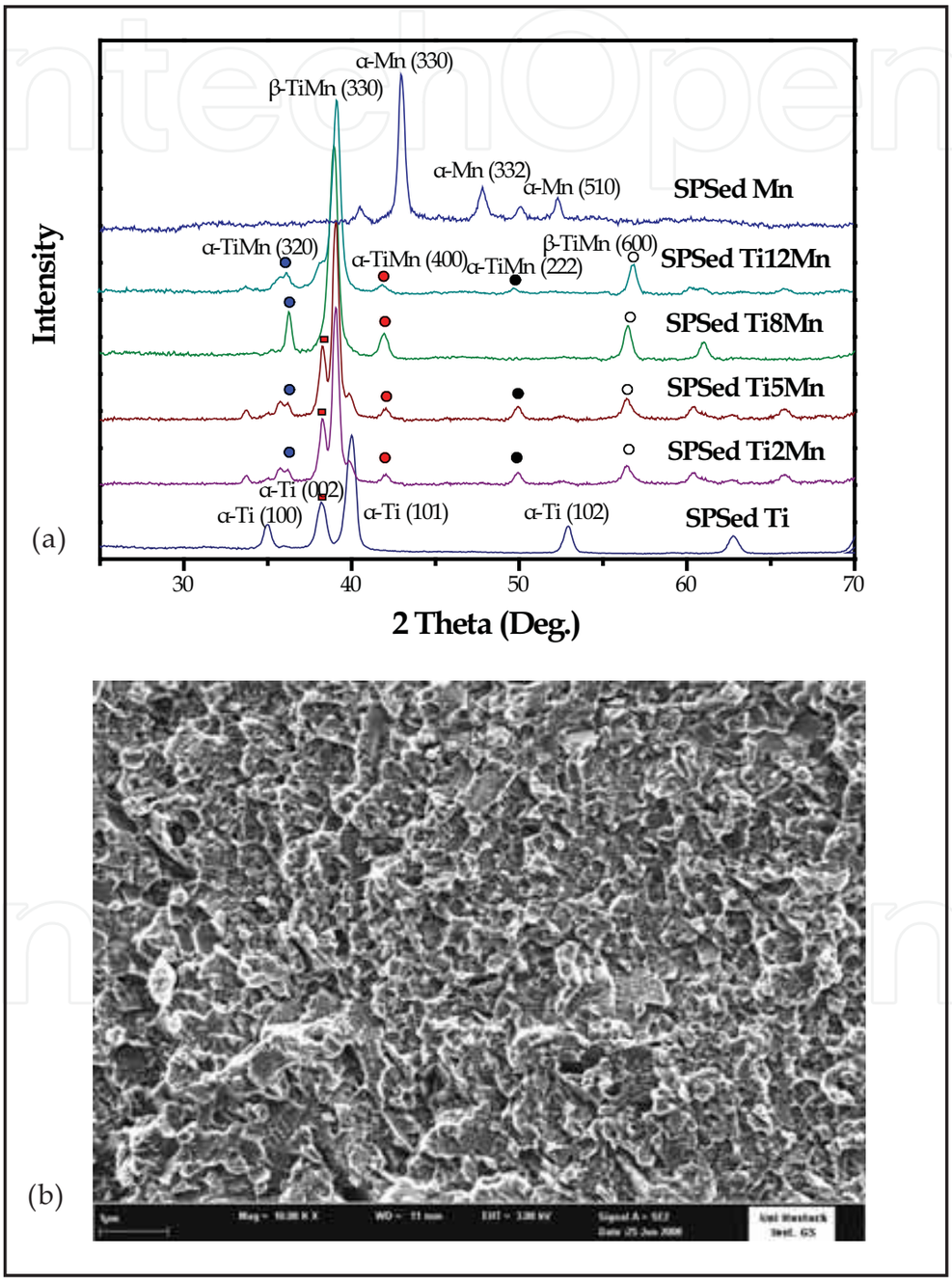

Fig. 4. XRD patterns of the spark plasma sintered Ti, Mn and TiMn alloys showing the TiMn alloys are α+β phase alloy (a) and SEM micrograph of the fracture surface of a Ti8Mn alloy.

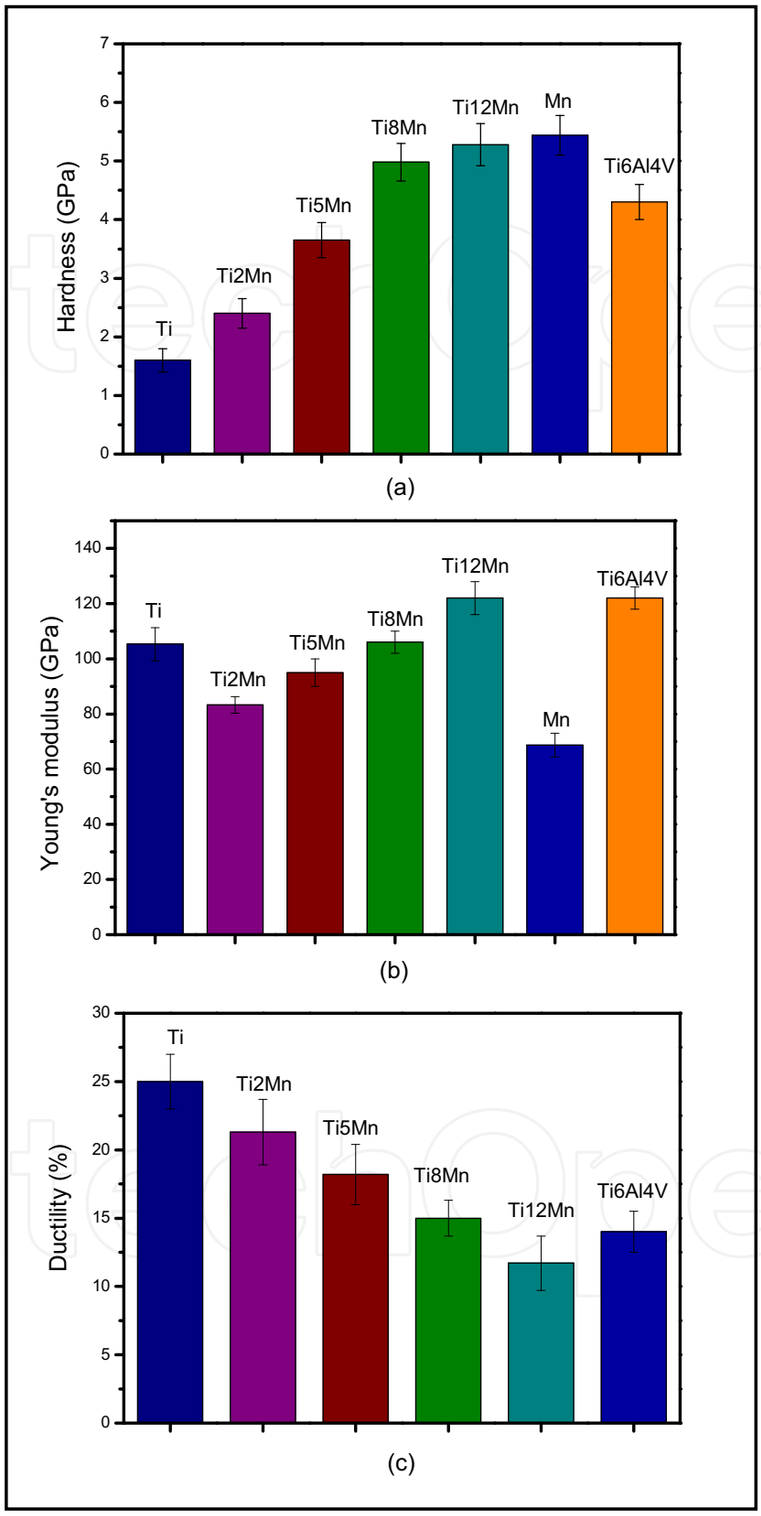

Fig. 5. Hardness (a) and Elastic modulus (b) of the Ti, Mn, TiMn and Ti6Al4V alloys obtained by microindentation tests, as well as ductility values at room temperature (c) of the TiMn alloys

The TiMn alloys provide higher hardness and elastic modulus than those of the pure Ti. The Ti5Mn and Ti8Mn alloys show comparable hardness but lower elastic modulus compared to the Ti6Al4V alloy. The increment of the hardness and elastic modulus of the TiMn alloys is ascribed to the formation α+β TiMn phases which are intermetallic phases with excellent mechanical properties. The Ti6Al4V alloy was chosen for orthopedic implant for several reasons. Excellent ductility is one of the most important reasons for its wide use in biomedical industry. The ductility of Ti6Al4V alloy is measured to be 14% at room temperature. The ductility of the TiMn alloy decreased from 21.3% (Ti2Mn) to 11.7% (Ti12Mn) with increase of Mn amount. However, the Ti2Mn, Ti5Mn, Ti8Mn alloys have higher ductility than that of the Ti6Al4V. Compared with the Ti6Al4V, the Ti2Mn alloy presents lower hardness (2.4 GPa) with better elastic modulus (83.3 GPa) and ductility (21.3%). The Ti5Mn alloy exhibits comparable hardness (3.65 GPa) and better elastic modulus (95.0 GPa) and ductility (18.2%) and the Ti8Mn alloy shows better hardness (4.98 GPa) and elastic modulus (106 GPa) with a comparable ductility (15.0%). In the light of their mechanical properties, the Ti2Mn, Ti5Mn and Ti8Mn alloys are suitable as biomedical implants.

Fig. 6 represents the cytotoxicity and cell proliferation results of the TiMn alloys. The tissue culture polystyrene (TCPS) was used as a control material. The MG-63 osteoblast cell viability (%) of the pure Ti and TiMn alloys by MTS assay is shown in Fig. 6(a). The cytotoxicity increases with increasing amount of the Mn contents in the Ti alloy. Cell's viability on pure Mn and Ti12Mn was about 50 % and 72 %, respectively ($p<0.05$). However, cells on the Ti5Mn and Ti8Mn alloys were also influenced concerning viability without statistical difference ($p>0.05$), but it reached comparative high values (89 %, 86 %, respectively) comparable with that of pure Ti (93 %). The proliferation of MG-63 osteoblasts on the TiMn alloys using flow cytometric cell proliferation analysis is demonstrated in Fig. 6 (b). The percentage of cells on the pure Ti and TiMn alloys decreases in contrast to the TCPS control (53.67 %). The number of proliferating cells on TiMn alloys (Ti2Mn 41.17%, Ti5Mn 40.50 %, Ti8Mn 41.57% and Ti12Mn 39.99 %) is reduced compared with that of pure Ti (48.93 %), however, with $p>0.05$ not significantly and all acceptable for biomedical applications. However, the percentage of proliferating cells grown on pure Mn is significantly reduced to 35.87 % ($p<0.05$). The student t-test, an established statistical method, shows that the proliferation of MG-63 osteoblast cells on TiMn alloys is not remarkably inhibited. Only Mn is significantly decreased ($p<0.05$). The decrease in pure Mn is about 27% from the Ti value. It is indicated that only a very high amount of Mn inhibits cell proliferation. Combining the cytotoxicity and cell proliferation results, leads to the assumption that the amount of Mn below 8 wt.% has a negligible effect on the cytotoxicity and cell proliferation of all tested Ti alloys.

Some commercial Ti alloys also contain Mn as an alloying component. The Mn has been doped in magnesium alloy with 1.2 wt. % and it was found that the Mn has no toxicity and can improve the corrosion resistance and mechanical properties of Mg (Xu et al., 2007). The Mn was doped to tri-calcium phosphate bioceramics and showed good cell compatibility (Sima et al., 2007). Recently, a Fe-35Mn alloy was prepared and showed higher strength and ductility, degradable properties. These observations make it suitable for biodegradable stent applications (Hermawan et al., 2007). The values concerning cytotoxicity and cell proliferation of the TiMn alloys demonstrate a dependency on the Mn concentration. A lower Mn content (<8 wt.%) in Ti has a low effect on the cytotoxicity and cell proliferation properties ($p>0.05$). In general, the Ti2Mn, Ti5Mn and Ti8Mn were comparable in viability

and cell proliferation properties with pure Ti. The Ti6Al4V alloy was firstly used in aerospace industry, and then applied in biomedical field as bone and dental implants. Until now, the Ti8Mn alloy as one of the typical α+β Ti alloys has been extensively used in aerospace industry because of its excellent mechanical properties. Our research here suggests that the application of the Ti8Mn alloy could be extended to biomedical field. As well as the Ti2Mn and Ti5Mn alloys, they exhibit higher ductility and lower elastic modulus than those of Ti6Al4V. The lower values of the elastic modulus of metals for joint prosthesis could decrease the stress-shielding effect in bone-implant coupling. The Ti2Mn, Ti5Mn and Ti8Mn alloys all exhibit acceptable cytotoxicity and cell proliferation of the human osteoblasts. Consequently, all the Ti2Mn, Ti5Mn and Ti8Mn alloys have a potential for the use in the biomedical field as new bone substitutes and dental implants.

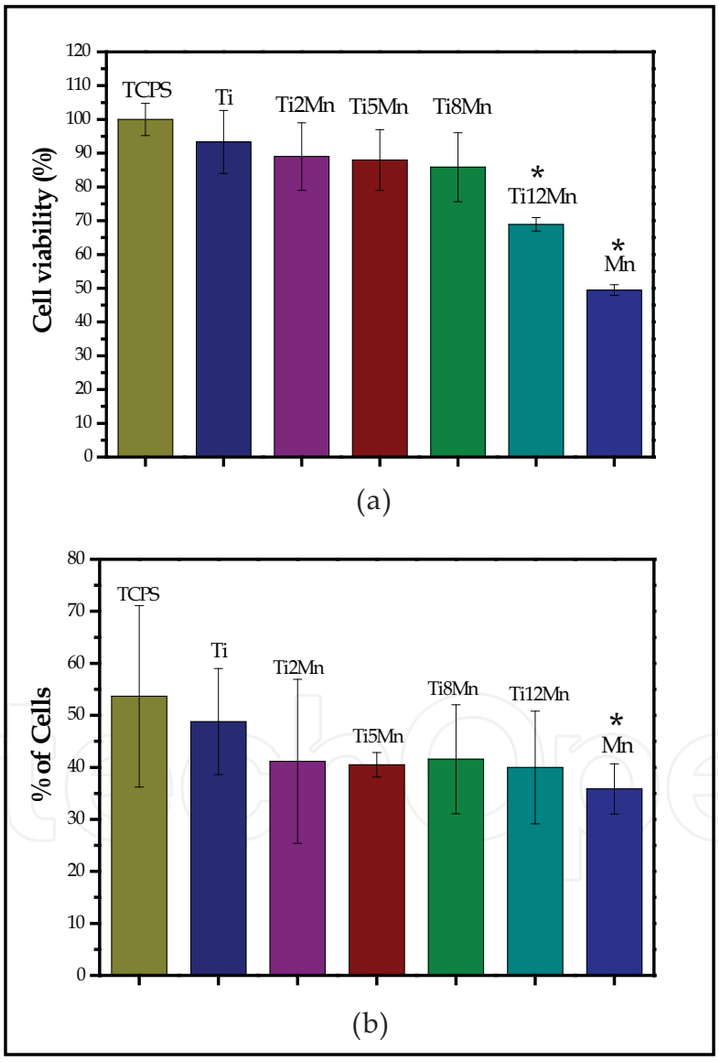

Fig. 6. Cytotoxicity (a) and cell proliferation (b) of MG-63 osteoblasts on the Ti and TiMn alloys showing the comparable cell viability of Ti2Mn, Ti5Mn and Ti8Mn alloys with that of pure Ti, and the proliferation of osteoblasts was not inhibited on TiMn alloys but only significantly on pure Mn. Mean ±SD, n=5, Student t-test * $p<0.05$.

4. Macroporous Titanium foams

4.1 Preparation and microstructures of the Titanium foams

High density pure Ti, and TiMn alloys were prepared by using the SPS in the above section. In this section, the preparation of Ti and TiMn foams by using the SPS will be introduced. Firstly, the pure Ti foams were prepared by the free pressureless SPS method developed by Zhang et al. (Zhang et al., 2008). The Ti powders were mixed with 15 wt. % of NH_4HCO_3 and 2 wt. % of TiH_2 powder as pore forming agents. Then the powder mixture was sintered at 1000°C by the SPS under a pressureless condition. Using 3D reconstruction by topographical methods is the most realistic way to get information on the internal structure of the foams in a non-destructive way. Fig. 7 shows the 3D reconstructions of the obtained Ti foams. The 3D cropped isometric view of cross sections in this Ti foam shows the non-uniform pore distribution and poor interconnectivity (Fig. 7a). The Micro-CT 2D top view and side views show that the macropore shapes are in irregular cross sections and randomly distributed (Fig. 7b-d). The 3D cropped internal surface exhibits pore size of 410 ± 90 μm. The XRD results indicate that these Ti foams by free pressureless SPS method are in β-Ti phase (Ibrahim, Zhang et al, 2011).

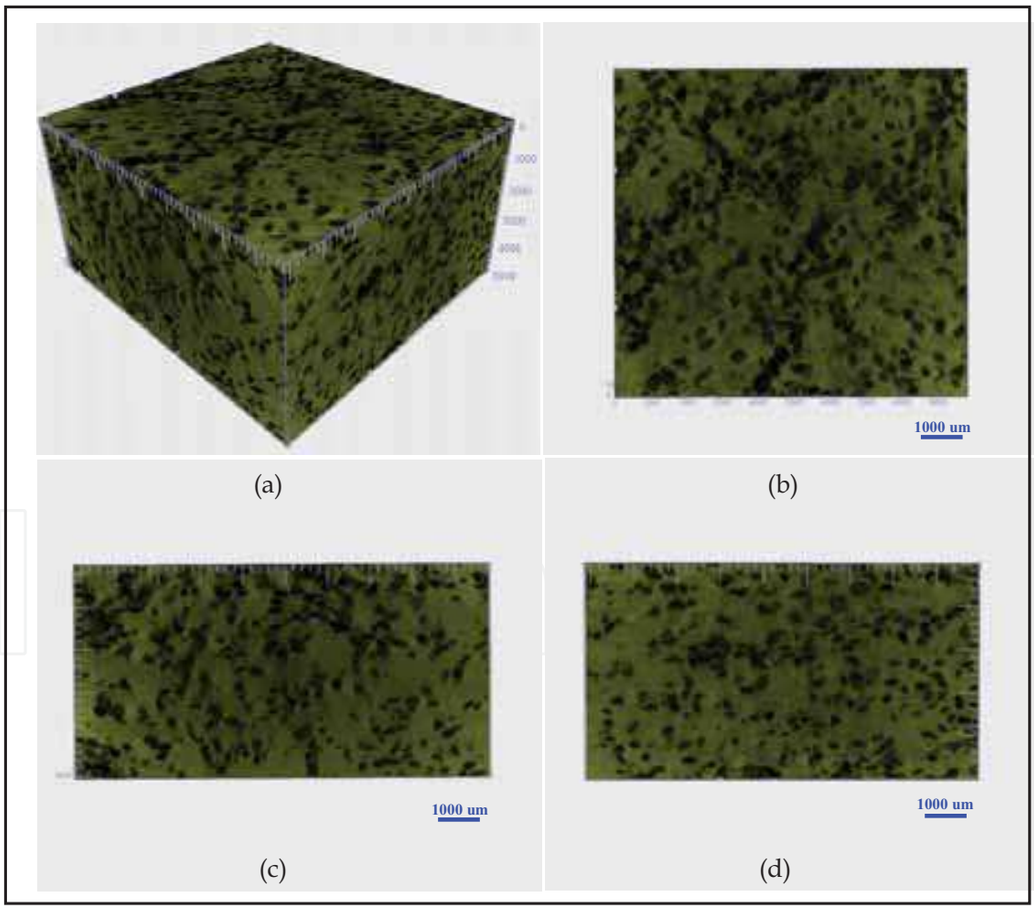

Fig. 7. Micro-CT 3D reconstructions of the Ti foam with NH_4HCO_3 and TiH_2 as pore forming agents produced at 1000°C by free pressureless SPS method with an isometric view (a), 2D top view (b), left side view (c), and right side view (d). Scale spacing, 1000 μm.

Alternatively, Ti foams with NaCl as spacer material were prepared at 700 °C by SPS under 50 MPa. Fig. 8 shows the 3D μ-CT reconstructions of the obtained Ti foams. This spark plasma sintered titanium foams shows 55% porosity and 250 μm pore size. The 3D cropped isometric view of cross sections in the Ti foam shows the uniform pore distribution and interconnected 3D porous structures with a high porosity (Fig. 8 a). The Micro-CT 2D top view and side views show that the macropore shapes are in square cross sections, uniform distribution of pore sizes with high interconnectivity (Fig. 8b-d). The 3D surface, the cell wall thickness and the connectivity were examined by the Micro-CT in a non-destructive way. The 3D cropped internal surfaces exhibit highly porous structures and interconnectivity with pore sizes of 243±50 μm and a cell wall average thickness of 20.4 μm. The XRD results indicate that these Ti foams are in α-Ti phase.

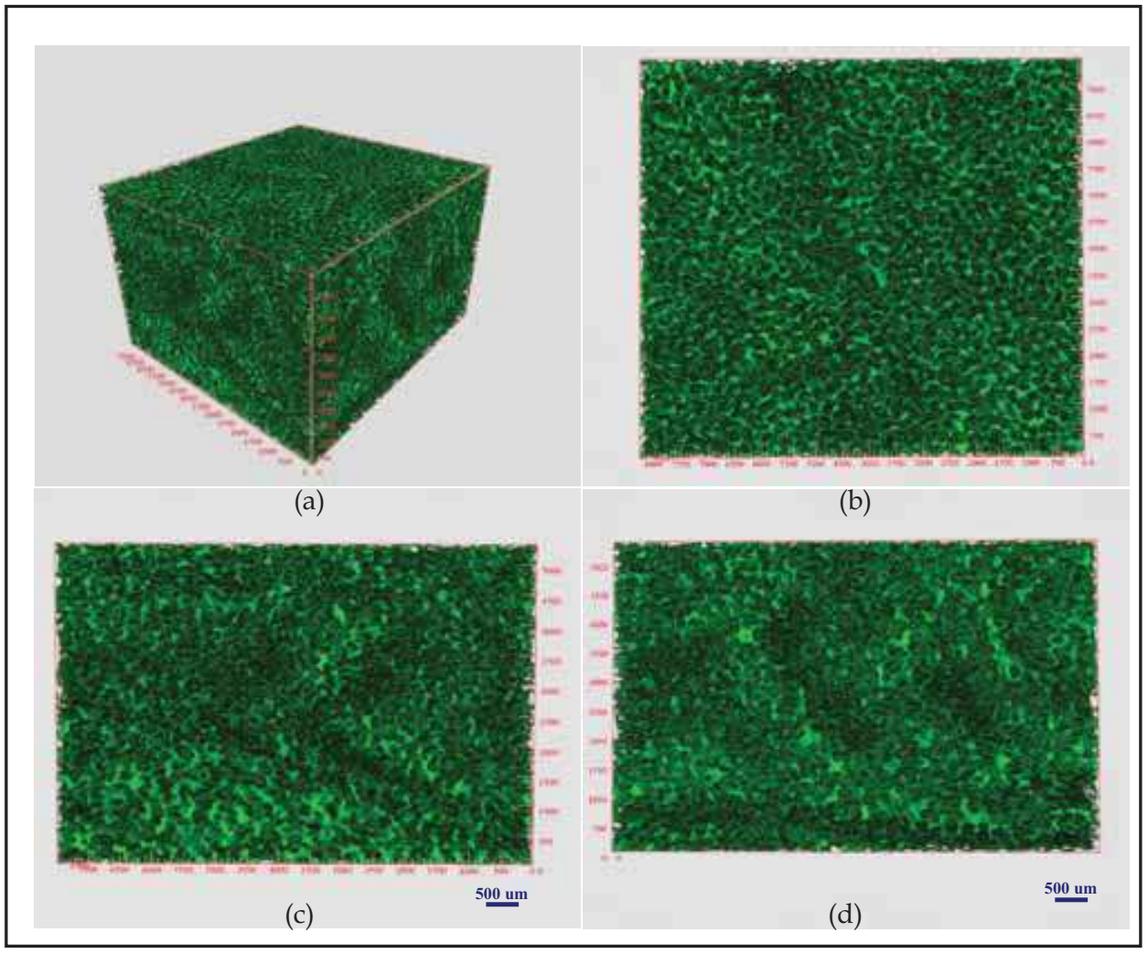

Fig. 8. Micro-CT 3D reconstructions of the Ti foam with NaCl as spacer material prepared by SPS at 700 °C under 50 MPa with an isometric view (a), 2D top view (b), left side view (c), and right side view (d). Scale spacing, 500 μm.

The results in Fig.7 and Fig. 8 indicate that the Ti foams have been prepared successfully by using the SPS technique. The foams prepared by the SPS and NaCl dissolution method show better interconnectivities than those prepared by the free pressureless SPS method. High

interconnectivity of the foams will support the osteconduction of bone tissue. Therefore, Ti foams with different pore sizes and porosities were prepared by the SPS and NaCl dissolution method. The influence of the weight ratio and particle size of NaCl on the porosity and pore size of Ti foams with corresponding SPS parameters is shown in Table 1. The pore sizes of the sintered foams were measured from the SEM images. This shows a mean pore size of about 125 μm in the foams with the NaCl spacing material being in the range of 88-149 μm, a mean pore size of 250 μm with NaCl of the sizes 224-297 μm, a pore size of 400 μm with NaCl of 388-500 μm sizes and a pore size of 800 μm with NaCl of 784-1000 μm sizes. After the porosity characterization by the Archimedes method, it was noticed that more NaCl particles were needed to obtain the same porosity in the large pore sized foams. To achieve a porosity of 55% in the 125 μm foams, the weight ratio of Ti:NaCl is about 1:1.28. However, the weight ratio of Ti:NaCl is about 1:1.75 in the 800 μm foams for the same porosity. This might be due to the decreased specific surface area in the large sized NaCl particles as spacer materials.

Ti powder	NaCl powder	Weight ratio (Ti: NaCl)	Porosity	Pore size	SPS parameters (Temperature, dwell time)
10-30 μm	88-149 μm (170-100 mesh)	1:1.28	~55%	~125 μm	700 °C, 8 min
10-30 μm	149-297 μm (100-50 mesh)	1:0.72	~30%	~250 μm	700 °C, 8 min
		1:0.93	~45%	~250 μm	700 °C, 8 min
		1:1.32	~55%	~250 μm	550 °C, 8 min
					600 °C, 8 min
					650 °C, 8 min
					700 °C, 8 min
					730 °C, 8 min
					750 °C, 5 min
					800 °C, 3 min
		1:1.64	~70%	~250 μm	700 °C, 8 min
10-30 μm	354-500 μm (45-35 mesh)	1:1.46	~55%	~400 μm	700 °C, 8 min
10-30 μm	707-1000 μm (25-18 mesh)	1:1.75	~55%	~800 μm	700 °C, 8 min

Table 1. The influence of the weight ratio and particle size of NaCl on the porosity and pore size of the Ti foams with corresponding SPS parameters.

The SEM micrographs of the Ti foams with the same porosity of 55% but different pore sizes of 125 μm, 250 μm, 400 μm, and 800 μm are shown Fig. 9. All the foams from 125 to 800 μm exhibit highly interconnected porous structures and uniform pore distributions. It is found

that the pores have irregular quadratic cross sections. They are similar to those of the initial NaCl particles of cuboid shapes.

Fig. 10 shows the SEM micrographs of the porous Ti foams with the same pore size of 250 μm with different porosities of 30 %, 45%, 55% and 70%. The thickness of the pore walls in the 30% porosity foams is about 100 μm, decreasing to 50 μm in 45% porosity foams, and to 20 μm in 55%, finally ending at 10 μm in 70% porosity foams. The interconnectivity was also enhanced with the increase in porosity. The 30% and 45% porosity foams show poor interconnectivity because of the lower porosity. But the 55% and 70% higher porosity samples show good interconnectivity. The macropores are in square cross sections in all the Ti foams with different porosities.

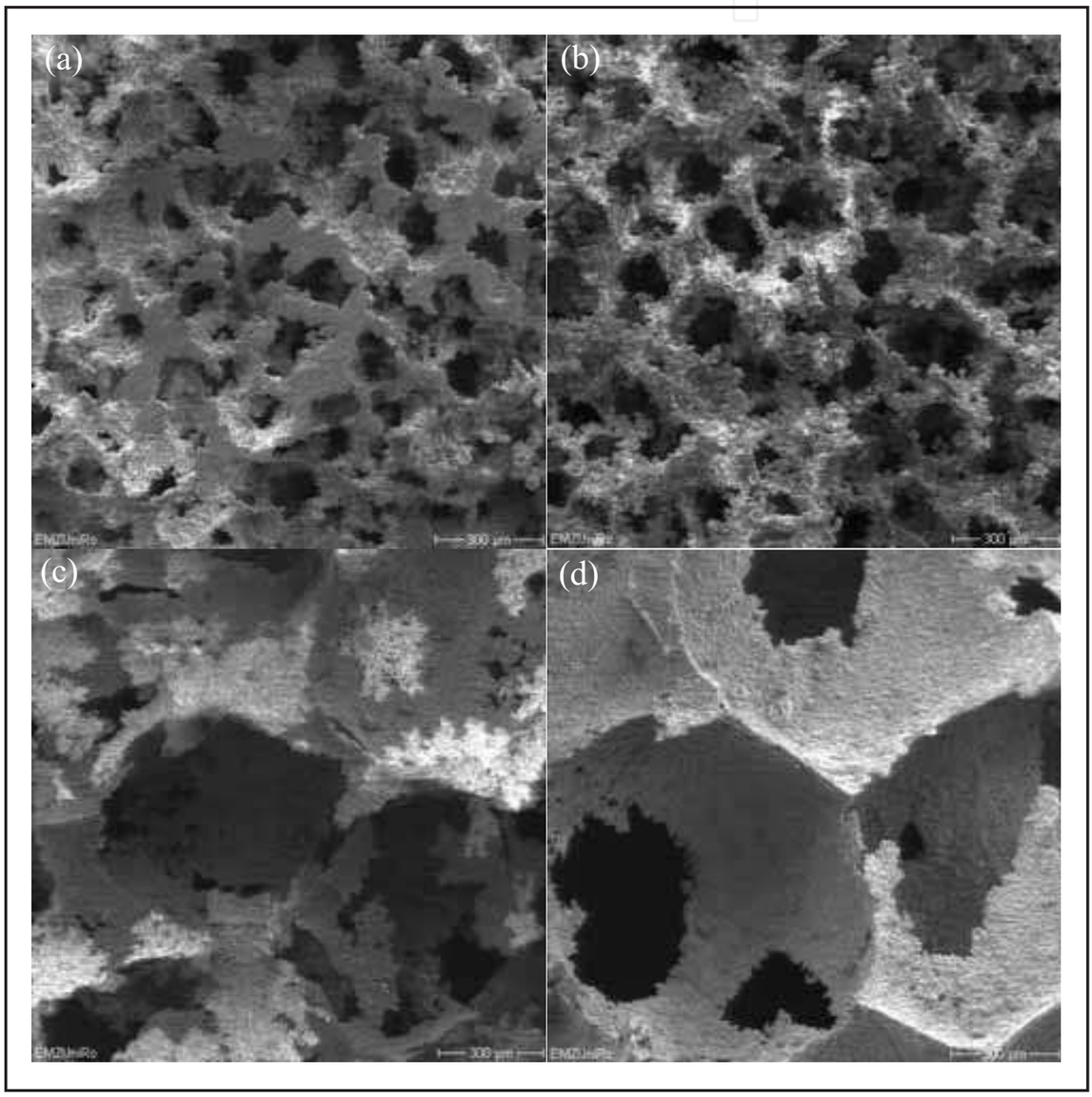

Fig. 9. SEM micrographs of the Ti foams with the same porosity of 55% but different pore sizes of 125 (a), 250 (b), 400 (c) and 800 μm (d). Scale bars, 300 μm.

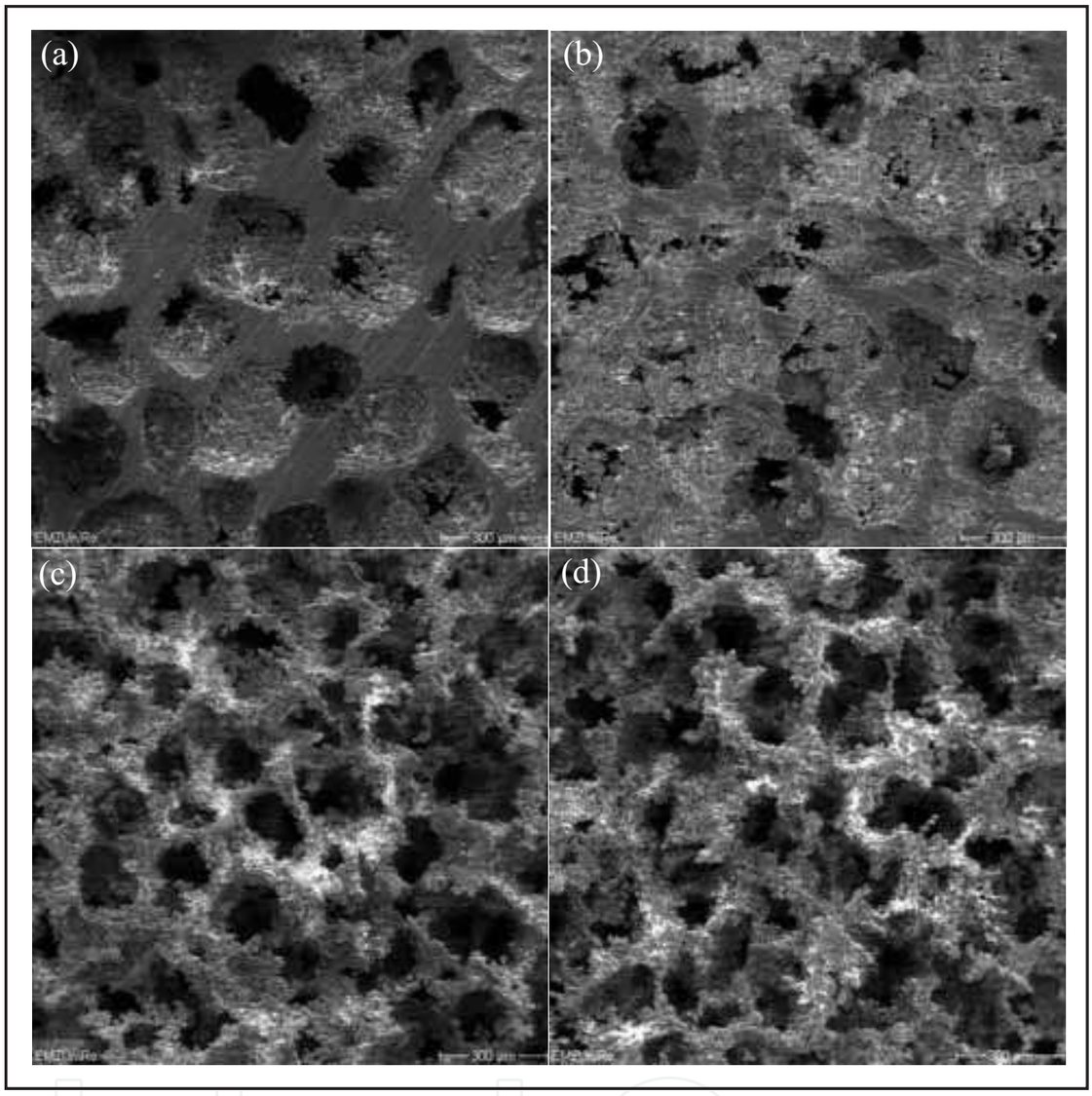

Fig. 10. SEM micrographs of the Ti foams with the same pore size of 250 μm but different porosities of 30 % (a), 45% (b), 55% (c) and 70% (d). Scale bars, 300 μm.

4.3 Mechanical properties of the Ti foams

Fig. 11 shows the effect of pore size and porosity on the plateau stress and Young's modulus of the porous Ti foams. The measured plateau stress and Young's modulus of the Ti foams were compared with values calculated following Gibson-Ashby model. According to the Gibson-Ashby model, the relationship between the relative plateau stress and relative density is given by (Wen et al., 2002):

$$\sigma/\sigma_0 = C\left(\rho/\rho_0\right)^{3/2} \tag{1}$$

where σ is the plateau stress of the foams, σ_0 is the yield stress of the dense material; C is a constant 0.3 from the data of cellular metals and polymers (Gibson & Ashby, 1997), ρ is the

density of the foams, ρ_0 is the density of the dense material. The density of the pure Ti is 4.5 g/ cm^3 with yield stress of 692 MPa (Long & Rack, 1998). The density of the Ti foam with 55% porosity and 250 μm pore size is 1.69 g/cm^3. Substituting these values in Equation 1, the theoretical value was calculated to be 47.78 MPa, which is comparable to the measured plateau stress 45.1±3.0 MPa.

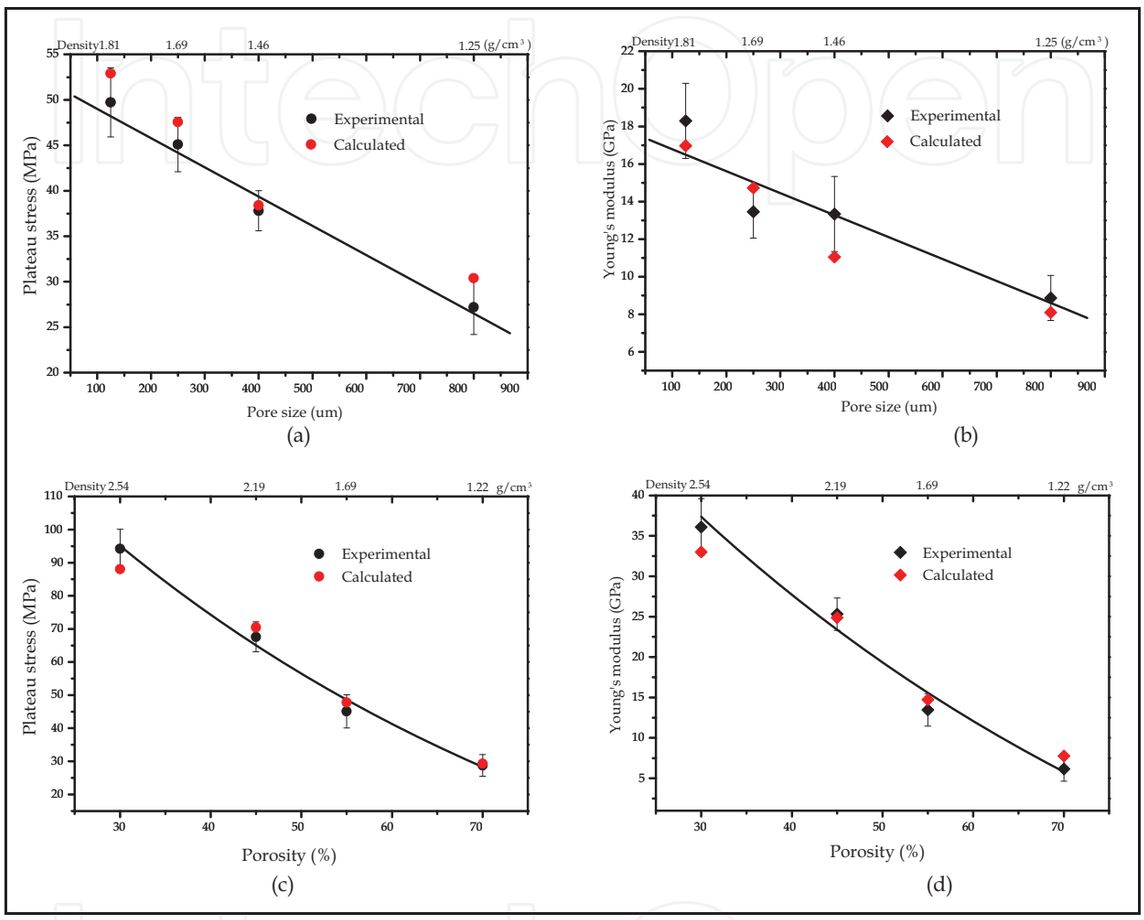

Fig. 11. The effects of pore sizes (a, b) and porosities (c, d) on the plateau stress and Young's modulus of the Ti foams.

According to the Gibson-Ashby model, the relationship between the relative Young's modules and relative density is given by (Wen et al., 2002):

$$E/E_0 = A(\rho/\rho_0)^2 \quad (2)$$

where E is the Young's modulus of the foams, E_0 is the Young's modulus of the dense materials, A is a constant of 1 including data of metals, rigid polymers, elastomers and glasses. The Young's modulus of the pure Ti is 105 GPa according to the Equation 2 (Long & Rack, 1998). The measured Young's modulus of the above Ti foams with 55% porosity is 13.46 GPa ± 1.4 GPa. Substituting the values into Equation 2, gives the theoretical value of 14.81 GPa which is also comparable to the measured one. All the Ti foams prepared by the SPS were measured and calculated.

As seen from the Fig. 11, it can be deduced that all the experimental data agree with the Gibson-Ashby model (1) and (2) in the present study. The relationship between the pore sizes and the mechanical properties of the Ti foams is shown in Fig. 11 (a, b). The plateau stress decreased from 49.7 MPa ±3.8 MPa to 27.2 MPa ± 3.0 MPa with the pore size increase (Fig. 11a). The Young's modulus reduced from 18.3 GPa ±2.0 GPa to 8.9 GPa ±1.5 GPa with the pore size increase (Fig. 11b). It coarsely obeys a linear decay with the pore size increase. The effect of the porosity on the mechanical properties of the Ti foams is shown in Fig. 11 (c, d). The plateau stress decreased from 94.2 MPa ± 5.9 MPa to 28.8MPa ± 3.3 MPa, and the Young's modulus decreased from 36.1 GPa ± 3.5 GPa to 6.2 GPa ± 1.8 GPa with porosity increase. It generally obeys the rule of exponential decline with the porosity increase.
The plateau stress and Young's modulus coarsely obey linear declines with the pore size increase and exponential decay with the porosity increase. Liu found that the plateau stress of the porous hydroxylapatite ceramics decreases linearly with increasing macropore size for a given total porosity (Liu, 1997). In this study, we found the plateau stress and Young's modulus coarsely obey linear declines with the pore size increase (Fig. 11 a, b). Rice RW has proposed a function for the relationship of the porosity and the strength of porous solids (Rice, 1993),

$$\sigma = \sigma_0 \exp(-cp) \tag{3}$$

where σ_0 is zero-porosity strength, σ is the strength at pore volume fraction p, and the constant c is related directly to the pore characteristics such as pore shape and size. In this study, we used the same Ti powder and NaCl spacer material; therefore, σ_0 and c can be considered as constant. According to the above function, the strength (σ) should decrease exponentially as the pore volume fraction (p) increases. Our results in Fig. 11 (c, d) are well in accordance with the above function.

4.4 Surface modification

Using the SPS and NaCl dissolution method, Ti8Mn foams were also prepared at SPS temperature of 700 ºC under 50 MPa. Fig.12 (a) shows the SEM micrograph of the Ti8Mn foams. It shows pore sizes of about 300 μm with interconnected pore distributions. The porosity of the Ti8Mn foam is 65% determined by the Archimedes principal method. These Ti8Mn foams process a compressive plateau stress of 68.5 MPa ± 13 MPa and an elastic modulus of 32.3 GPa ± 1.8 GPa. Additionally, the obtained TiMn foams were surface modified by immersing in a NaOH solution at 60 ºC for several hours. The foams were washed and heat treated at 600 ºC (Takemoto, 2006). The SEM micrographs of a Ti8Mn foam sample with a surface modified by TiO_2 nanostructures are shown in Fig. 12 (b-d). The micrographs at different magnifications show that oriented nanowire structures cover all the surfaces of the pore walls in the TiMn foams. The X-ray diffraction results confirmed the surface TiO_2 nanostructures as anatase/rutile phases.
Finally, the in vitro bioactivity of surface modified Ti8Mn foams was tested by suspending in polystyrene bottles containing simulated body fluid solution at 37.0°C in a shaking bath. At certain times, the samples were taken out, rinsed with deionized water, and dried in an oven. The results show that these anatase/rutile phases of the TiO_2 nanostructures on the Ti8Mn foams have very high *in vitro* bioactivity. They formed apatite (hydroxyapatite) on the pore walls of the Ti8Mn foams after only 3 days soaking in the simulated body fluid (Fig.13). The EDX analysis indicates the precipitation of bone-like biomimetic apatite. The

deposition of the apatite on the pore walls is a biomineralization process where the TiO_2 nanostructures provide proper nucleation sites. This high *in vitro* bioactivity of the TiO_2 modified Ti8Mn foams indicates a high bone-bonding ability of these foams *in vivo*.

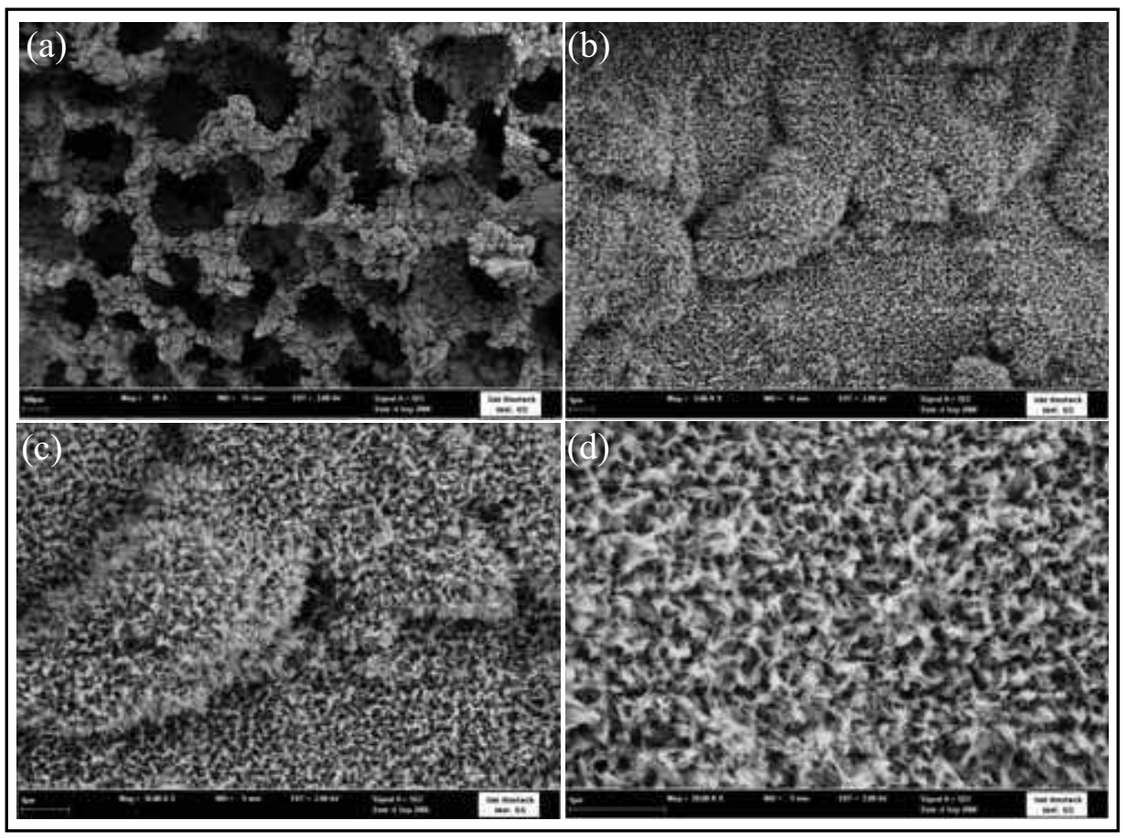

Fig. 12. SEM micrograph of the Ti8Mn foams prepared by the SPS and NaCl dissolution method (a), and morphologies of the surface modified TiO_2 nanostructures on the porous wall of the foams at different magnifications (b-d).

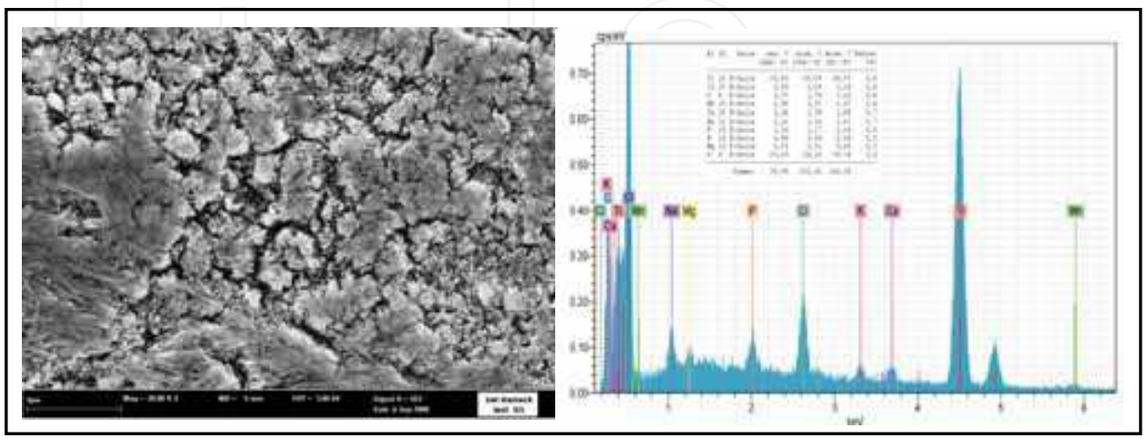

Fig. 13. SEM micrograph (a) and EDX (b) of the TiO_2 modified Ti8Mn foam immersed in simulated body fluid for 3 days showing the apatite formation.

Implants sometimes were used to substitute bone defects in tumour or spine surgery. Porous Ti and its alloy foam with their osteoconductive properties are an ideal alternative bone graft. The porous structure with pore sizes of 200-500 μm of the Ti foams may be able to permit bone cell penetration and tissue integration. The plateau stress of the human vertebral bone (load-bearing site) ranges from 24 to 43 MPa, and femoral cancellous bone (load-bearing site) is in the range of 48-80 MPa (Zhang et al, 2007). The average Young's modulus of compact bone of human ranges 7-30 GPa (Zhang et al, 2007). The plateau stress of the presented Ti and Ti8Mn foams in the range of 27-94 MPa is comparable to that of the cancellous bone which is sufficient for biomedical applications. For biomedical applications, the main problem of Ti and Ti alloys in clinical view is their high Young's modulus. Stress shielding is known to lead to bone resumption and eventual loosening of the implant. The dense Ti generally showed much higher Young's modulus (70-120 GPa) than that of human bone. Thus, the porous structures were incorporated in the Ti and Ti alloys. In this study, the porous Ti and Ti8Mn foams show lower Young's modulus values (6.2-36.1 GPa) than that of dense ones which are comparable to those of natural compact bone (7-30 GPa). The macroporous Ti and Ti8Mn foams with plateau stress 27.2-94.2 MPa and Young's modulus 6.2-36.1 GPa have a potential to be used as bone implants. The low Young's modulus of titanium foams is desirable to reduce the amount of stress shielding of the bone into which the foam is implanted. Thus, the good biocompatibility, the interconnected porous structure achieved by the SPS and the NaCl dissolution method and the observed mechanical properties comparable to those of human bones make pure Ti and Ti8Mn foams to ideal bone implant materials.

5. Conclusions and outlook

The α+β type TiMn alloys with high relative density and ultrafine microstructures were prepared by using mechanical alloying for 60 hours and spark plasma sintering at 700 °C for 5 min. The Mn reduced the α to β transformation temperature of Ti and was confirmed as a β stabilizer element. The hardness increased significantly ranging from 2.4 GPa (Ti2Mn) to 5.28 GPa (Ti12Mn), the elastic modulus ranging from 83.3 GPa (Ti2Mn) to 122 GPa (Ti12Mn) and the ductility decreased ranging from 21.3% (Ti2Mn) to 11.7% (Ti12Mn) with increasing manganese content in the Ti. Concentrations of Mn below 8 wt.% in titanium reveal negligible effects on the metabolic activity and the cell proliferation of human osteoblasts. Therefore, the Mn could be used in lower concentrations as an alloying element for biomedical titanium. The Ti2Mn, Ti5Mn and Ti8Mn alloys all have a potential for use as new bone substitutes and dental implants.

Macroporous Ti foams were successfully fabricated by the free pressureless SPS technique. Micro-CT results showed the non-uniform pore distribution and poor interconnectivity in these foams. Alternatively, macroporous pure Ti foams with porosities of 30-70% and pore sizes of 125-800 μm were prepared by using SPS and NaCl dissolution method. The Ti foams prepared by SPS at 700 °C for 8 min under 50 MPa showed pure α-Ti phase structure. The Ti foams consist of interconnected macropores with square cross sections. The plateau stress and Young's modulus agree with the Gibson-Ashby models, and coarsely obey linear declines with the pore size increase and exponential decays with the increase of porosity. Ti8Mn foams were also prepared in α+β phases with a porosity of 65% and pore sizes of 300 μm by using the SPS and NaCl dissolution method. TiO_2 nanostructures in anatase/rutile phases were modified on the pore walls of the Ti8Mn foam uniformly by NaOH solution

soaking and heat treatment. This surface modified TiMn foam exhibited high *in vitro* bioactivity with a fast apatite-forming ability in the simulated body fluid. The Ti and Ti8Mn foams processed by SPS and NaCl dissolution method showed mechanical properties within those of human bone range making these materials to be ideal bone implant foams.

As load bearing and long term hard tissue repair materials, Ti and its alloys are the most outstanding metallic materials nowadays. The modification (processing and/or surface) of the clinic used Ti alloys, and the exploration of new Ti alloy systems for biomedical applications are still the tasks for the future. For the Ti foams, the development of processing techniques to create controlled porosity, pore sizes and interconnectivity is still required. The relationship between the relative density and mechanical properties of the Ti foams can be predicted well with the Gibson-Ashby model. However, the relationships between the porosity-functional properties (thermal, flow, transport, absorption and so on) are not well modelled yet. The effects of pore architecture, pore size, pore interconnectivity, inter-connective pore size on the mechanical and functional properties of Ti foams are still not clear, and need more investigations. Energy saving is one of the hot issues in 21st century. There are high requirements of new sintering techniques with rapid energy transfer and less energy consumption to produce dense Ti alloys and foams. The SPS is considered as a novel field sintering technique for fast preparation of diverse bulk materials with a near net shape. The future highlights will be the preparation of nanostructured Ti alloys and the processing of Ti foams with complex shapes by using the SPS technique. The application of the SPS in preparation of the biomedical Ti alloys and foams has perspective future.

6. Acknowledgements

Funding for this research was supported by the DFG-Deutschen Forschungsgemeinschaft (German Research Foundation) with grant No. GRK1505/1 (Welisa). The authors acknowledge the group of PD Dr. Barbara Nebe in Department of Cell Biology of Rostock University for the help in the cell experiments, and the group of PD Dr. Ulrich Beck in Department of Electrical Engineering and Informatics of Rostock University for the help in the SEM experiments.

7. References

Barbieri, F.C.; Otani, C.; Lepienski, C.M.; Urruchi, W.I.; Maciel, H.S.; Petraconia, G. (2007). Nanoindentation study of Ti6Al4V alloy nitrided by low intensity plasma jet process. *Vacuum*, 67: 457–461.

Brown, S.E. (2006). Bone Nutrition, In: *Scientific Evidence for Musculoskeletal, Bariatric, and Sports Nutrition*, Editor: Ingrid Kohlstadt, CRC Press, ISBN: 978-0849337246, US.

Gao, L.; Wang, H.Z.; Hong, J.S.; Miyamoto, H.; Miyamoto, K.; Nishikawa, Y.; Torre, S.D.D.L.(1999). Mechanical properties and microstructure of nano-SiC-Al2O3 composites densified by spark plasma sintering. *Journal of the European Ceramic Society*.19(5): 609-613.

Geetha, M.; Singh, A.K.; Asokamani, R.; and Gogia, A.K. (2009). Ti based biomaterials, the ultimate choice for orthopaedic implants – A review. *Progress in Materials Science*, 54: 397-425.

Gibson L. J. & Ashby M.F. (1997). *Cellular solids: structure and properties*. Cambridge University Press, ISBN: 0-521-49560-1.UK.

Gu, Y.W.; Khor, K.A.; Cheang, P. (2004). Bone-like apatite layer formation on hydroxyapatite prepared by spark plasma sintering (SPS). *Biomaterials*. (25)18: 4127-34.

Hermawan, H.; Dube, D.; Mantovani, D. (2007). Development of degradable Fe-35Mn alloy for biomedical applications. *Advanced Materials Research*.15-17: 107-122.

Ibrahim, A; Zhang, F; Otterstein, E.; and Burkel, E. (2011). Processing of porous Ti and Ti5Mn foams by spark plasma sintering. *Materials & Design*. 32(1):146-153.

Jayaseelan, D. D.; Kondo, N.; Brito, M.E.; Ohji, T. (2002). High-strength porous alumina ceramics by the pulse electric current sintering technique. *Journal of the American Ceramic Society*. 85(1): 267-269.

Li, J.P.; Li, S.H.; Van Blitterswijk, C.A.; de Groot, K. (2005). A novel porous Ti6Al4V: characterization and cell attachment. *JBiomed Mater Res A*, 73: 223-233.

Liu, D.M. (1997). Influence of porosity and pore size on the compressive strength of porous hydroxyapatite ceramic. *Cera. Inter*. 23: 135-139.

Long, M.; Rack, H. J. (1998). Titanium alloys in total joint replacement—a materials science perspective. *Biomaterials*. 19, 1621-1639.

Lou, Y.; Pan, W.; Li, S.; Wang, R.; Li, J. (2003). A novel functionally graded materials in the Ti-Si-C system. *Materials Science and Engineering A*. 345(1-2):99-105.

Mark, J.J.; & Waqar, A. (2007). *Surface Engineered Surgical Tools and Medical Devices*, Springer, ISBN: 978-0-387-27028-9, US.

Munir, Z. A.; Anselmi-Tamburini, U. (2006). The effect of electric field and pressure on the synthesis and consolidation of materials: A review of the spark plasma sintering method. J Materials Science. 41:763–777.

Nicula, R.; Cojocaru, V.D.; Stir, M.; Hennicke, J.; Burkel, E.. (2007). High-energy ball-milling synthesis and densification of Fe–Co alloy nanopowders by field-activated sintering (FAST). Journal of Alloys and Compounds, 434-435: 362-366.

Nicula, R.; Lüthen, R.; Stir, M.; Nebe, J.B.; Burkel, E. (2007). Spark plasma sintering synthesis of porous nanocrystalline titanium alloys for biomedical applications. *Biomolecular Engineering*. 24: 564-567.

Nicula, R.; Turquier, F.; Stir, M.; Kodash, V.Y.; Groza, J.R.; Burkel E. (2007). Quasicrystal phase formation in Al–Cu–Fe nanopowders during field-activated sintering (FAST). *Journal of Alloys and Compounds*. 434-435: 319-323.

Rice, R.W. (1993). Comparison of physical property-porosity behaviour with minimum solid area models. *J Mater. Sci*. 8: 2187-2190.

Sima, F.; Socol, G.; Axente, E.; Mihailescu, I.N.; Zdrentu, L.; Petrescu, S.M.; Mayer, I. (2007). Biocompatible and bioactive coatings of Mn2+-doped β-tricalcium phosphate synthesized by pulsed laser deposition. *Applied Surface Science*. 254: 1155-1159.

Takemoto, M.; Fujibayashi, S.; Neo, M.; Suzuki, J.; Matsushita, T.; Kokubo, T.; Nakamura, T. (2006). Osteoinductive porous titanium implants: effect of sodium removal by dilute HCl treatment. *Biomaterials*. 27:2682-2691.

Wen, C. E.; Yamada, Y.; Shimojima, K.; Chino, Y.; Asahina, T.; Mabuchi, M. (2002). Processing and mechanical properties of autogenous titanium implant materials. *J Mater. Sci.: Mater. Med*. 2002,13, 397-401.

Xu, L. P.; Yu, G.; Zhang, E.; Pan, F.; Yang, K. (2007). In vivo corrosion behavior of Mg-Mn-Zn alloy for bone implant application. *JBiomed Mater Res A*. 83: 703–711.

Zhang, F.; Shen, J.; Sun, J. (2004). The Effect of Phosphorus additions on Densification, Grain growth and Properties of nanocrystalline WC/Co composites. *Journal of Alloys and Compounds*. 385(1-2): 96-103.

Zhang, F.; Shen, J.;Sun,J.; Zhu, Y.Q.;Wang, G.; and McCartney, G. (2005) Conversion of Carbon Nanotubes to Diamond by a spark plasma sintering. *Carbon*. 43 (6): 1254-1258.

Zhang, F.; Chang, J.; Lu, J.; Lin, K.; and Ning, C. (2007). Bioinspired structure of bioceramics for bone regeneration in load-bearing sites. *Acta Biomaterialia*, 3(6): 896-904.

Zhang, F.; Lin, K.; Chang, J.; Lu, J.; and Ning, C. (2008). Spark plasma sintering of macroporous calcium phosphate scaffolds from nanocrystalline powders. *Journal of the European Ceramic Society*. 28 (3): 539-545.

Zhang, F.; Weidmann, A.; Nebe, B. J. ; Burkel, E. (2009) . Preparation of TiMn alloy by mechanical alloying and spark plasma sintering for biomedical applications. *Journal of Physics: Con. Series*. 144: 012007.

Zhang, F.; Weidmann, A.; Nebe, J.B.; Beck, U.; Burkel., E. (2010). Preparation, microstructures, mechanical properties, and cytocompatibility of TiMn alloys for biomedical applications. *JBiomed Mater Res Part B,Appl Biomater*, 94: 406–413.

Zhang, F.; Otterstein E.; Burkel E. (2010). Spark plasma sintering, microstructures and mechanical properties of macroporous titanium foams. *Advanced Engineering Materials*. 12(9): 863-872.

Biomedical Engineering, Trends in Materials Science

Edited by Mr Anthony Laskovski

ISBN 978-953-307-513-6
Hard cover, 564 pages
Publisher InTech
Published online 08, January, 2011
Published in print edition January, 2011

Rapid technological developments in the last century have brought the field of biomedical engineering into a totally new realm. Breakthroughs in materials science, imaging, electronics and, more recently, the information age have improved our understanding of the human body. As a result, the field of biomedical engineering is thriving, with innovations that aim to improve the quality and reduce the cost of medical care. This book is the second in a series of three that will present recent trends in biomedical engineering, with a particular focus on materials science in biomedical engineering, including developments in alloys, nanomaterials and polymer technologies.

InTech Europe
University Campus STeP Ri
Slavka Krautzeka 83/A
51000 Rijeka, Croatia
Phone: +385 (51) 770 447
Fax: +385 (51) 686 166
www.intechopen.com

InTech China
Unit 405, Office Block, Hotel Equatorial Shanghai
No.65, Yan An Road (West), Shanghai, 200040, China
中国上海市延安西路65号上海国际贵都大饭店办公楼405单元
Phone: +86-21-62489820
Fax: +86-21-62489821

IntechOpen